Available online at www.sciencedirect.com
SCIENCE DIRECT
ELSEVIER
European Journal of Mechanics B/Fluids 25 (2006) 505–531
EUROPEAN JOURNAL OF MECHANICS B/FLUIDS

A criterion for detection of the onset of Dean instability in Newtonian fluids

H. Fellouah, C. Castelain, A. Ould El Moctar, H. Peerhossaini *

Thermofluids, Complex Flows and Energy Research Group, Laboratoire de Thermocinétique, UMR CNRS 6607, Polytech Nantes, Rue Christian Pauc, B.P. 90604, 44306 Nantes cedex 3, France

Received 26 June 2005; received in revised form 21 October 2005; accepted 11 November 2005

Available online 18 January 2006

Abstract

Dean instability for Newtonian fluids in laminar secondary flow in 180° curved channels was studied experimentally and numerically. The numerical study used Fluent CFD code to solve the Navier–Stokes equations, focusing on flow development conditions and the parameters influencing Dean instability. An accurate criterion based on the radial gradient of the axial velocity was defined that allows detection of the instability threshold, and this criterion is used to optimize the grid geometry. The effects on Dean instability of the curvature ratio (from 5.5 to 20) and aspect ratio (from 0.5 to 12) are studied. In particular, we show that the critical value of the Dean number decreases with the increasing duct curvature ratio. The variation of the critical Dean number with duct aspect ratio is less regular.

In the experimental study, flows were visualized in several tangential positions of a 180° curved channel with aspect ratio 8 and curvature ratio 10. The flow is hydrodynamically developed at the entrance to the curved channel. The critical Dean number is detected and the development of secondary flow vortices by additional counter-rotating vortex pairs is observed. A diagram of different critical Dean numbers is established.

Keywords: Dean instability; Centrifugal instability; Hydrodynamic stability; Curved channel; Secondary flow; Experimental study; Numerical study

1. Introduction

Since curved channels provide compactness, high heat and mass-transfer rates, transverse mixing and an extended laminar flow regime (Peerhossaini [1]), they are widely used in turbomachinery and in heat exchangers for heating/cooling systems. Detailed knowledge of the secondary flow in curved channels is crucial for better understanding and control of the flow in the chaotic advection regime generated in a succession of alternating ±90° elbows (Castelain et al. [2]).

Curvature in ducts generates a centrifugal force outward from the center of curvature. An imbalance between this force and the pressure gradient in the flow field generates a secondary flow as a pair of counter-rotating sym-

* Corresponding author. Tel.: +33 2 40 68 31 40; fax: +33 2 40 68 31 41.
E-mail address: hassan.peerhossaini@univ-nantes.fr (H. Peerhossaini).

0997-7546/$ – see front matter
doi:10.1016/j.euromechflu.2005.11.002

Nomenclature

a	width of the channel cross-section
b	height of the channel cross-section
D_h	hydraulic diameter
De	Dean number
f	force
g	gravitational body force
$i,\ j,\ l$	nodal point
$L_{dev.}$	axial development length
p	static pressure
Rc	mean curvature radius
$u,\ v,\ w$	horizontal, vertical and axial velocity components
Um	mean velocity
$x,\ y,\ z$	Cartesian coordinates

Greek symbols

θ	angular position in the curved channel
ν	kinematic viscosity
ρ	density
τ	the shear stress tensor

metrical vortices, called corner vortices, in the duct cross-section. Beyond a critical value of Dean number De ($De = (UmD_h/\nu)\sqrt{D_h/Rc}$, where Um is the mean velocity, ν the kinematic viscosity, D_h the hydraulic diameter and Rc the mean radius of curvature), another pair of counter-rotating vortices, called Dean vortices, appears on the outer (concave) wall of the duct. These vortices are due to Dean instability, one of the large family of centrifugal instabilities of which Taylor–Couette and Görtler instability are also members [1]. One must however pay attention to not confuse between the *Corner vortices* and the Dean vortices. Corner vortices are due to a non-equilibrium state caused by an imbalance between the centrifugal force and viscous force and appear on the end walls. They are called corner vortices by Moffatt [3], end cells or Ekman vortices by Finlay and Nandakumar [4]. The *Dean vortices* develop along the concave wall beyond a critical Dean number and are due to an instability mechanism.

Steady fully developed laminar Newtonian curved flows of circular cross-section have been studied extensively; some previous work is presented in Berger et al. [5]. The first solution to the flow in curved tubes was suggested by Dean [6], who solved the axisymmetric laminar flow problem and demonstrated the existence of secondary flow. This secondary flow was observed experimentally by Eustice [7] by injecting ink into water flowing through a coiled pipe, and was confirmed later by White [8]. The perturbation method has been shown to be valid for small values of the Dean number, and hence this method has been adopted by many authors (Ito [9], Cuming [10]) as the first step in the numerical investigation of flow in curved ducts. The first investigation of flow in curved ducts of rectangular cross-section was made by Ito [9].

For high Dean numbers, many authors have used analytical approaches to the fully developed laminar flow problem. They assumed that the secondary flow and the mean velocity gradient due to the viscous effects were concentrated in thin layers along fixed boundary layers and that the flow outside these boundary layers was inviscid (Ito [11] for circular pipes, Mori et al. [12] for square pipes). To overcome this limiting assumption for high and intermediate Dean numbers, Cheng et al. [13], Ghia and Sokhey [14], Hwang and Chao [15] and Joseph et al. [16] obtained numerical solutions for developed laminar flow in square or rectangular ducts that predicted a second vortex pair near the concave wall for certain Dean numbers. Near the concave wall, where the axial velocity is decreasing to zero, is a centrifugally unstable region. If the axial velocity becomes large enough, viscous effects can no longer hold the two-vortex structure in place; thus the additional vortices appear. The flow is known to be unstable there due to the centrifugal instability. In the central region of the curved duct, the radial pressure gradient across the channel is positive (inward) but the centrifugal force decreases from its maximum value to zero at the concave wall. The instability is caused by the imbalance between the inwards pressure gradient and the outwards centrifugal force. The flow near the inner (convex) wall is stable. Cheng and Akiyama [17] presented a numerical solution, for steady fully developed laminar flow and convective heat transfer, in curved rectangular channels with aspect ratios 0.2, 0.5, 1, 2 and 5.

Baylis [18], Mori et al. [12] and Humphrey et al. [19] made experimental studies of the flow in curved square ducts and described the structure of the secondary flow. These studies used the Dean number as the only parameter to characterize the secondary flow and the appearance of the second vortex pair.

Cheng et al. [20] reported a visualization study of fully developed laminar flow in curved rectangular ducts for cross-section aspect ratios b/a of 1, 2, 3, 4, 5, 6, 8, 10 and 12 for curvature ratio $a/Rc = 0.2$ and for $b/a = 12$ with $a/Rc = 0.025$. They showed that further vortices are set up in addition to the main secondary flow vortices and that

the critical Dean number depends on the aspect and curvature ratios. The number of additional vortex pairs depends on the aspect ratio and the Dean number.

Sugiyama et al. [21] reported a flow visualization investigation of fully developed laminar flow in curved rectangular channels. The channels had aspect ratios ranging from 0.5 to 2.5, curvature ratios ranging from 5 to 8, and width 20 mm. They showed the development of the secondary flow vortices versus Dean number; the critical Dean number takes minimum and maximum values at aspect ratios of about 1 and 2, respectively.

Chandratilleke and Nursubyakto [22] presented a numerical simulation of secondary flow characteristics in flow through curved rectangular ducts of aspect ratios 1 to 8 and for Dean numbers in the range 20 to 500. They reported also that the number of Dean vortices formed is strongly influenced by the duct aspect ratio and the Dean number.

Ligrani and Niver [23] carried out a flow visualization study of Dean vortex flow for Dean numbers from 109 to 602 using a curved channel with aspect ratio 40 and inner to outer radius ratio 0.979. Their observations and photographs show several pairs of counter-rotating Dean vortices for Dean numbers above 175 and angular positions larger than 125°. In the same geometry, Ligrani et al. [24] showed that for a Dean number of 334 the instability starts at the angular position of 95°.

In the presence of instability, in addition to the corner vortices that exist naturally, another pair of counter-rotating vortices appears on the concave channel wall. In the literature, the criterion for the onset of the instability is visual, i.e. the visual detection of the appearance of the Dean vortices (Sugiyama et al. [21], Bara et al. [25]). However, visualization is only an approximative method for detection of instability.

The aim of this work is to develop an accurate and quantitative criterion for the detection of the threshold of Dean instability in curved channel flows. The rest of the paper is organized as following. Sections 2 and 3 respectively describe the numerical methodology and the experimental apparatus and methods used in this investigation. It should be recalled here that mesh optimization is carried out on the profiles of the radial gradient of the axial velocity which are used as the discriminator in the criterion for the detection of the instability. Therefore, mesh optimization is described in the corresponding section. Section 4 is devoted to the presentation of the results. In Sections 4.1 and 4.2 we focus on the flow structure and we compare experimental and numerical images of the flow with and without Dean instability. In particular, we show that the computer code used in this study is able to produce the unstable flow structures, but cannot predict (by helicity contour lines) accurately the instability threshold. Critical Dean number predicted by the code depends much on the resolution of the iso-value lines selected for visualization of the flow structure. This fact warrants the search for a quantitative criterion for the detection of the threshold of Dean instability. This criterion is developed in Section 4.3.1. With this criterion developed, in Sections 4.3.2–4.3.5 we examine the effects of curvature ratio, cross-section aspect ratio and the angular position on the critical Dean number. Then in Section 4.4 the code is used to characterize the global flow (basic flow and instability effects together) in curved channels of different cross-sections. Section 5 gives the conclusion.

2. Numerical methodology

The Fluent CFD solver was used to solve the time-independent three-dimensional Navier–Stokes equations governing an incompressible flow in a curved channel of rectangular cross-section. These equations are:

1. Equation of continuity:

$$\frac{\partial}{\partial x_i}(u_i) = 0 \tag{1}$$

2. Equations of motion in i direction:

$$\rho \frac{\partial}{\partial x_j}(u_i u_j) = -\frac{\partial p}{\partial x_i} + \frac{\partial \tau_{ij}}{\partial x_j} + \rho g_i + F_i, \tag{2}$$

$i, j = 1, 2, 3$ for the three-dimensional flow.

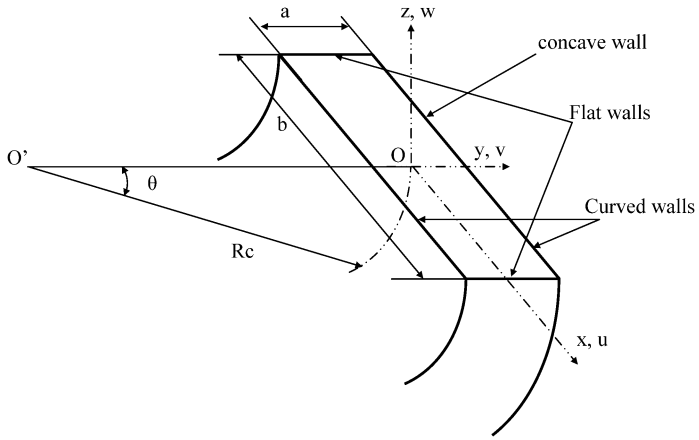

Fig. 1. Coordinates system.

u_i is the ith component of velocity, ρ is the fluid density, ρg_i and F_i are the gravitational body force and external body forces in the i direction respectively, p is the static pressure and τ_{ij} is the shear stress tensor for an incompressible flow given by:

$$\tau_{ij} = \mu\left(\frac{\partial u_i}{\partial x_j} + \frac{\partial u_j}{\partial x_i}\right) \tag{3}$$

where μ is the fluid viscosity.

Fig. 1 shows the coordinate system used to study the curved rectangular channels. The cross-section of the channel is a rectangle of width b and height a; b/a is the aspect ratio. The mean radius of curvature is Rc and Rc/D_h is the curvature ratio. Velocity components in the x, y and z directions are designated by u, v and w respectively. We call flat mid-plane, the planes which pass by the center of the canal cross section ($x = 0$) and are parallel to the flat walls. Also curved mid-plane, are the planes which pass by $y = 0$ and are parallel to the curved walls. The dimensions of the curved ducts studied are given in Table 1.

Because of channel symmetry, we imposed a symmetry condition to decrease the computation capacity for the large geometries ($b/a \geqslant 8$); we thus limit the geometry to a half cross-section.

The boundary conditions are:

$$u = 0, \quad v = 0, \quad w = 0 \quad \text{for } x = \pm b/2, \text{ and } y = Rc \pm a/2.$$

Of the several algorithms that Fluent proposes to solve the Navier–Stokes equations, we chose that with the segregated solver (this is the solution algorithm in which the governing equations are solved sequentially) to iterate the nonlinear partial differential equations, since this solver is better adapted to the large grids as in our work. To calculate pressure at the nodes we chose the body-force-weighted scheme, which works well when inertial forces are not negligible. Fluent uses the equation of continuity to deduce the pressure necessary to resolve the equations of motion. The Simplex algorithm was chosen for pressure–velocity coupling in order to obtain the pressure in the continuity equation. For the momentum equation, we used the Quick scheme (second order) because it is recommended in the presence of rotating flows. The Gambit program was used to generate the grid or mesh for the Fluent CFD solver.

Calculations start at a straight channel upstream of the curved duct. At the entry of the straight channel, an uniform velocity profile equal to the mean velocity is imposed. At the channel exit, the flow is hydrodynamically developed and enters the curved duct. Convergence is controlled by following the evolution of the residues for the velocity components and the continuity equation. For the velocity components, the residues represent the sum on all grid cells of the difference between the value of a variable calculated in one cell and that calculated by applying the conservation equation in the neighboring cells. For the continuity equation, the residues represent the ratio of the mass flow rate in a given iteration to the maximum mass flow rate in the first five iterations. In the convergence, the evolution residues must converge toward small (in all cases less than 10^{-6}) and stable quantities. The time necessary to reach the convergence is different, it depend on curvature ratio and aspect ratio.

Table 1
Dimensions of the curved channels used in the numerical study

b/a	Rc/D_h	Rc (m)	a (m)	b (m)
0.5	10	0.135	0.02	0.01
1	20	0.4	0.02	0.02
	15	0.3	0.02	0.02
	12	0.24	0.02	0.02
	10	0.20	0.02	0.02
	8	0.16	0.02	0.02
	5.5	0.11	0.02	0.02
	3.5	0.07	0.02	0.02
	2.5	0.05	0.02	0.02
2	10	271	0.02	0.04
3	10	0.30	0.02	0.06
4	10	0.32	0.02	0.08
5	10	0.34	0.02	0.1
6	10	0.35	0.02	0.12
7	10	0.36	0.02	0.14
8	20	0.71	0.02	0.16
	15	0.53	0.02	0.16
	12	0.43	0.02	0.16
	10	0.36	0.02	0.16
	8	0.28	0.02	0.16
	5.5	0.20	0.02	0.16
	2.5	0.09	0.02	0.16
12	10	0.37	0.02	0.24

3. Experimental setup

A water tunnel facility was specifically designed and constructed to provide well controlled flow through the test section. The test facility, an open-loop tunnel, is shown schematically in Fig. 2. Flow, generated by a volumetric pump from the tank to the test section, passes through a series of development elements before entering the test section. It first enters a diffuser. A 2.6 meter PVC straight duct is provided at the diffuser exit for relaxation of the flow streamlines and development of Poiseuille flow, and also to assure stable and clean inlet conditions. After the straight channel, the flow enters the test section, which consist of a 10 cm straight channel, a curved channel with curvature angle 180° and curvature ratio 10, and finally a 10 cm straight channel. The test section was made of Plexiglas to facilitate flow visualization and has a cross-section of 2 cm × 16 cm, giving an aspect ratio of $b/a = 8$, a large aspect ratio chosen to minimize the influence of side walls. Fully developed laminar flow in this case is reached for $L_{\text{dev.}}/(ReD_h) < 0.04$ (Muchnik et al. [26]). A 20 cm PVC straight channel was connected at the exit of test section to eliminate any effect of the adapter (rectangular–circular) on the flow at the duct exit.

The flow was visualized by the laser-induced fluorescence (LIF) technique (Peerhossaini and Wesfreid [27]). The flow is illuminated by a blue laser light (a 5 watt argon ion laser source) at a wavelength of 488 nm; the reemitted light is green, of about 514 nm wavelength. Fluorescein solutions of mass concentration 1 mg/l were used, so that density variation in the working fluid due to tracer addition is negligible. Dye is injected with a syringe upstream of the settling chamber; the tracer is distributed in the whole section. This kind of injection allows overall visualization (Castelain et al. [2]).

The secondary flow was visualized by illuminating the channel cross-section by a laser sheet. For this purpose, a traversing mechanism was constructed in which the relative position of the camera and the laser light sheet is fixed. The traversing mechanism rotates around the center of curvature of the bend under investigation and scans the flow at different angular positions. Fig. 3 shows the traversing mechanism and the camera orientation for viewing the illuminated plane at a 90° angle relative to the light sheet. A fluid of refraction index close to that of Plexiglas is injected between the lens surface and the bend outer wall to compensate for the material changes in the optical path. The cross-sections of the flow are viewed by a Dalsa camera equipped with Schneider optics. It is crucial that images taken in different streamwise sections of the flow be totally comparable from the optical point of view.

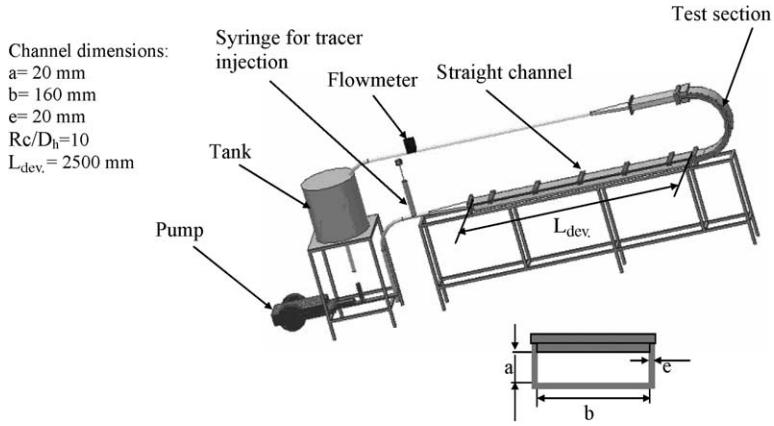

Fig. 2. Schematic of curved channel apparatus.

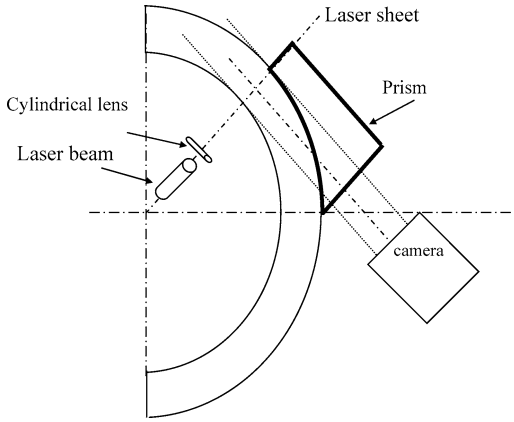

Fig. 3. Laser Induced Fluorescence (LIF) technique.

Images viewed by the camera are transferred directly to a digital image-processing system where they can be recorded and analyzed with a personal computer.

4. Results and interpretations

4.1. Evolution of the secondary flow at different angular positions

Fig. 4 shows the flow visualization images obtained at $De = 220$ for different observation locations from 60 to 180° of the entrance to the curved channel. The concave and the convex walls are respectively at the top and the bottom of each photograph. These visualizations are compared to the numerical visualizations, given by the helicity contour lines at each angular position. The helicity is defined by the dot product of vorticity and the velocity vector, it is given by the following relation:

$$H = \left(\nabla \times \vec{V}\right) \cdot \vec{V} \tag{4}$$

It provides insight into the vorticity component aligned with the fluid stream. Vorticity is a measure of the rotation of a fluid elements as they move in the flow field.

The first photograph in Fig. 4, corresponding to the 60° position, shows two symmetrical corner vortices located near the flat end walls. In the center part of the test section no vertical flow is visible. As remarked above, these two corner vortices exist naturally in the curved flow and Dean instability is not yet present. The helicity contour lines confirm the configuration of the corner vortices given by visualization at this position.

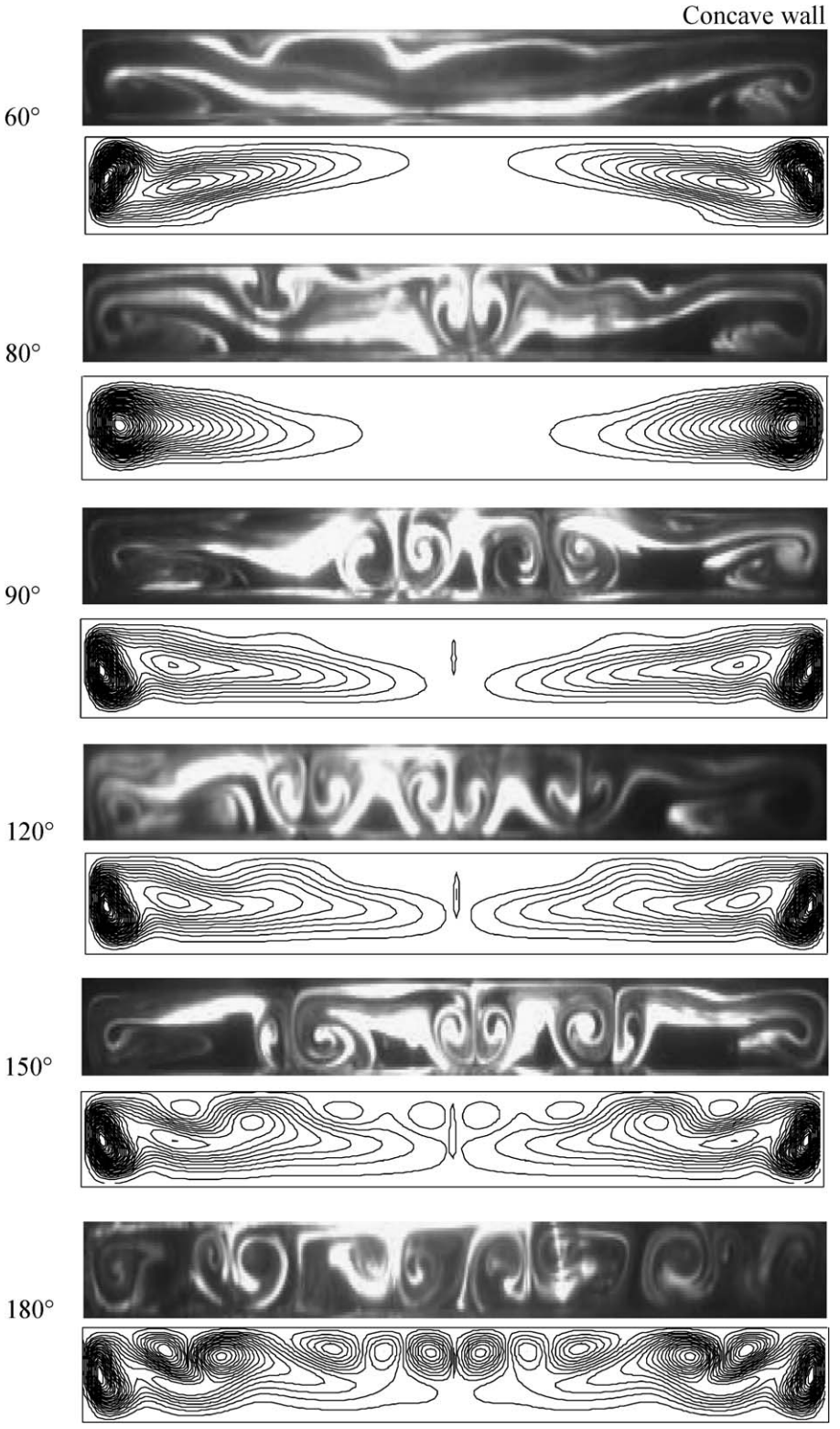

Fig. 4. Flow visualization observed at different cross-section of the curved channel at $De = 220$.

At the 80° position, the flow patterns have changed in the flow visualization image: in addition to the two corner vortices confined near the flat walls, a pair of Dean vortices appears in the central region due to the centrifugal instability in the flow.

At the 90° position, two pairs of counter-rotating vortices are clearly developed in the center of the cross-section and occupy the whole channel height. At 120°, the number of Dean vortex pairs grows to three, remaining unchanged at 150°. Contour-lines of helicity show that the flow is more disturbed at the position 150° than in 120°. At positions 90 and 120°, contour lines of helicity show no Dean vortex. At the curved channel exit (180°), Fig. 4 shows a flow with four pairs of Dean vortices in addition to the two corner vortices. The dark mushroom 'stems' with bright flanks on each side of each vortex are associated with the up-wash regions emerging from the concave wall between the two vortices in each pair of Dean vortices. The mushroom 'petals' correspond to the vortex core regions. It can be noted that the Dean vortices seem less developed in the numerical results: they remain more confined close to the concave walls, whereas in experiments they occupy quickly the full channel height.

4.2. Secondary flow for different Dean numbers

Fig. 5 presents the secondary flow patterns at the exit of the 180° curved rectangular channel for different Dean numbers. For low Dean numbers, from 65 to 127, only one pair of counter-rotating symmetrical cells near the flat walls is observed experimentally. Contour lines of helicity show that at $De = 115$, the corner vortices leave place for the Dean vortices which are visible at $De = 130$. At $De = 135$, two additional pairs of counter-rotating vortices appear in the center plane of the section. When the Dean number is further increased to 140, the number of additional pairs of counter-rotating vortices increases to three. This situation remains unchanged until $De = 200$. From this Dean number on, the entire channel is filled with the Dean vortices. This flow pattern is marked by the presence of four pairs of Dean vortices, a pattern not predicted in previous work: Thangam and Hur [28] and Chandratilleke and Nursubyakto [22] numerically predicted only three pairs of Dean vortices in this configuration.

Numerical and experimental development of these vortices are similar to those shown on Fig. 4; they develop more quickly and occupy all the section in the experimental study. On the other hand, in the numerical experiments an increase of the Dean number increases the number of vortices to reach six pairs for $De = 400$, whereas it is difficult to observe clearly more than four pairs of Dean vortices in the experimental results. This shows the delicacy of the comparison between experimental and numerical visualizations: experimentally, a certain number of disturbances affect the flow that are not taken into account numerically.

From Fig. 5, the contour lines show that for Dean numbers 115 and below, no Dean instability vortex is visible. A closer look at the numerical visualization results shows that these vortices are rather sensitive to the selected number of helicity contour lines. Thus, for a Dean number of 90 and with 30 iso-value helicity lines, no vortex is observed (Fig. 6(a)), whereas for 200 iso-value lines two vortices are seen (Fig. 6(b)). This sensitivity is generally inherent in the presentation of results in terms of iso-value lines. In fact, the more iso-value lines one put in the presentation, the more details one will capture. As there is no precise limit to the number of iso-value lines necessary to capture the real flow structure, therefore criteria based on iso-value lines suffer from lack of objectivity. This illustrates the real need for a accurate quantitative criterion for the detection of the instability threshold. Therefore, in the next sections we focused on the elaboration of a criterion for the detection of the threshold of Dean instability in curved channel flows.

4.3. Dean instability

Dean instability is a centrifugal instability appearing in Poiseuille flow in curved channel. There is no study, to the best of our knowledge, that gives the critical Dean number for the appearance of Dean vortices in curved channels of finite width. Reid [29] studied, for the first time, flow stability in a curved channel of rectangular cross-section. Because of the complexity of the analysis, he assumed that the flow in a curved channel could be represented by flow between two concentric cylinders. The stability diagram he obtained had critical Dean number 36. Reid's study [29] and that of Dean [30] concern the appearance of the basic secondary flow but not of the Dean instability.

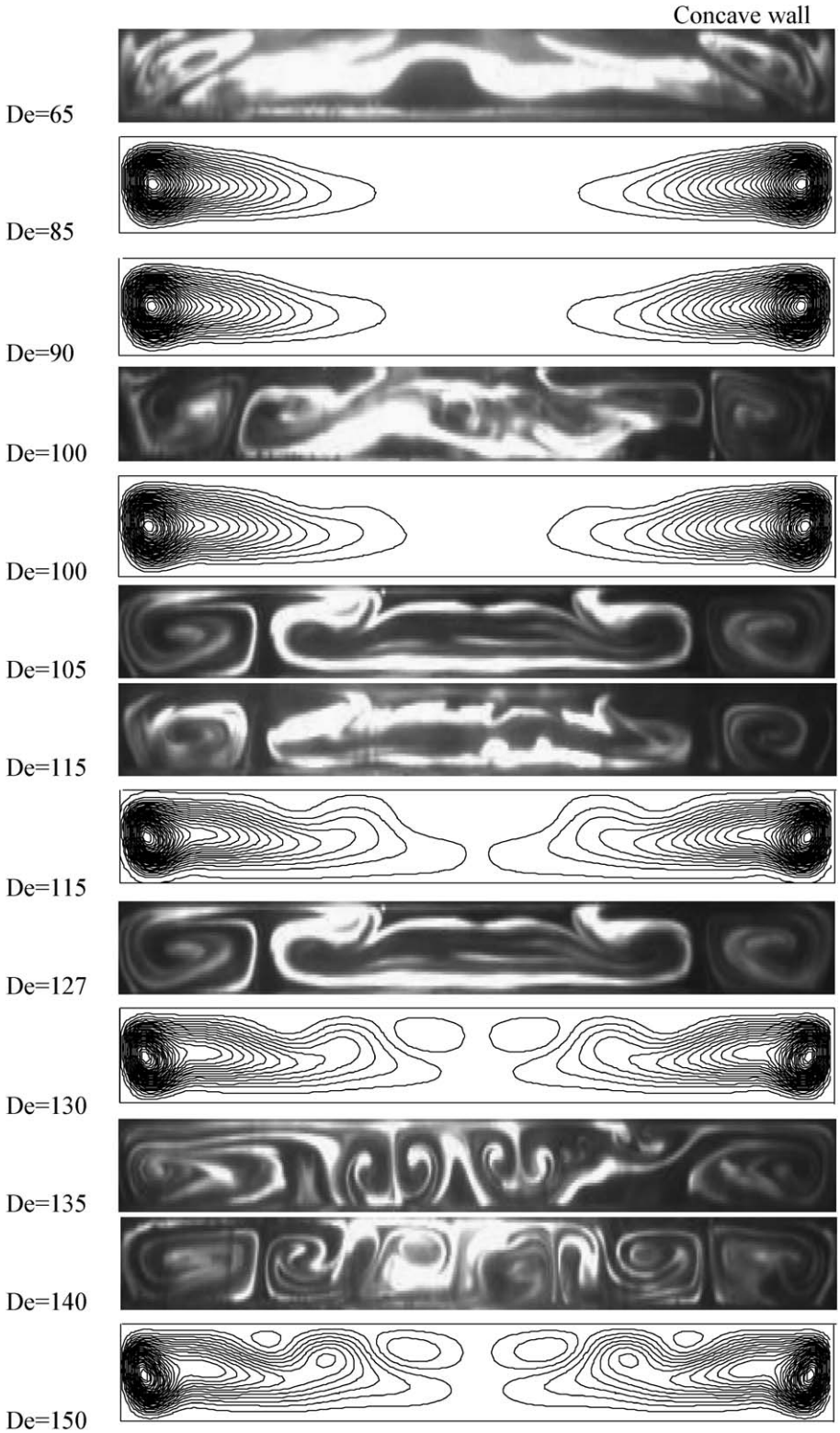

Fig. 5. Evolution of the flow structure observed 180° from the start of curvature.

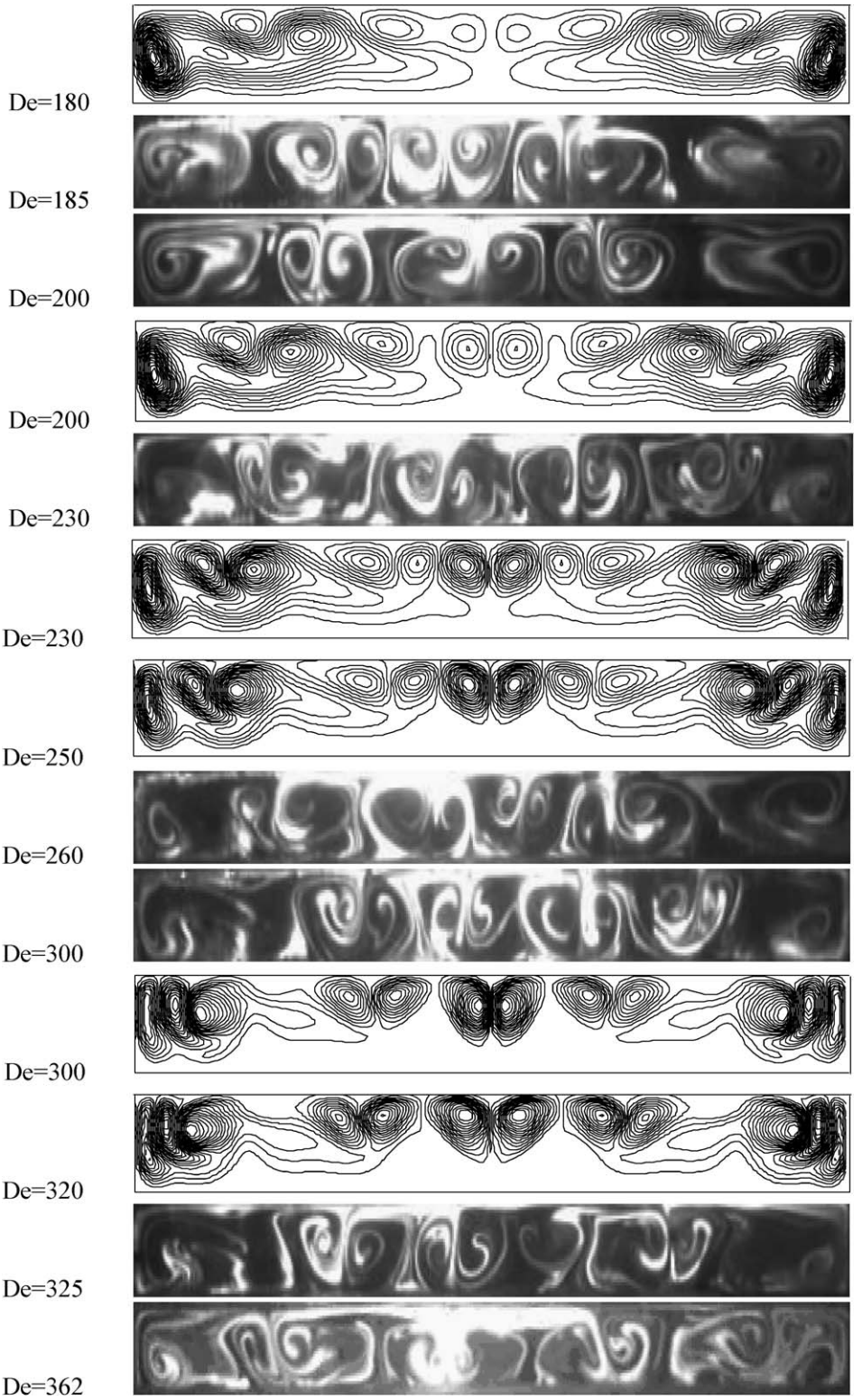

Fig. 5 (*continued*).

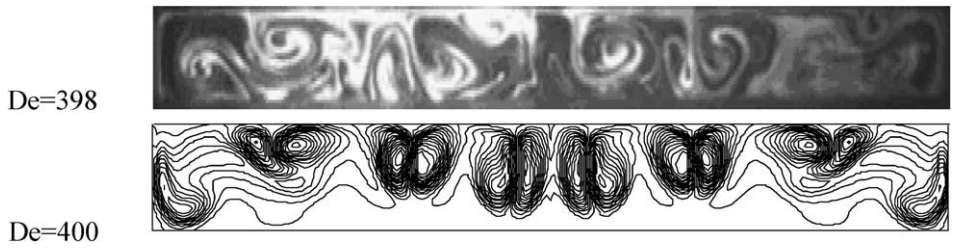

Fig. 5 (*continued*).

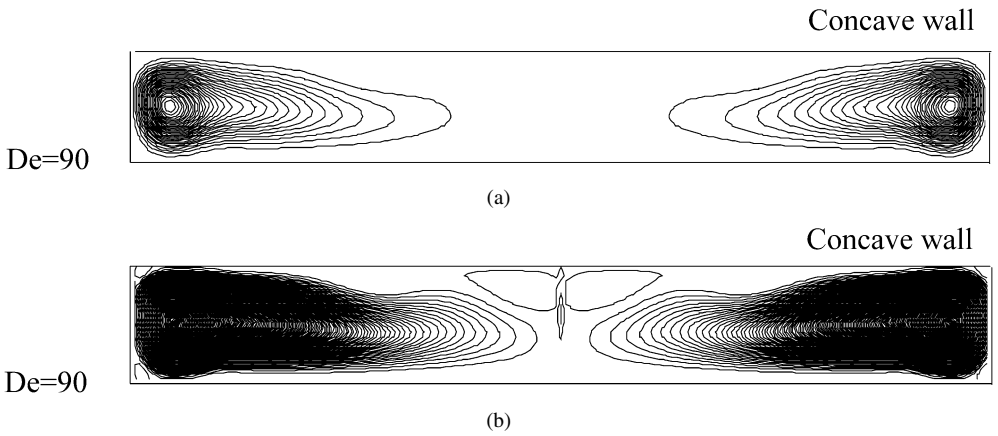

Fig. 6. Flow structures observed at position of 180°, $Rc/D_h = 10$. (a) The number of contours lines is 30, (b) the number of contours lines is 200.

4.3.1. A criterion for detection of the onset of Dean instability

We suggest here an accurate and reliable criterion for detection of Dean instability. The secondary flow in a curved duct consists of a pair of counter-rotating symmetrical vortices; the corner vortices. Beyond a critical Dean number, another pair of counter-rotating vortices appears on the concave wall of the duct, as shown in Fig. 7. The question is how to calculate the critical Dean number for the appearance of this new pair of vortices, or equivalently how to detect the passage from flow with two corner vortices to flow with four cells (two corner vortices and two Dean vortices).

As remarked above, the commonly accepted criterion in the literature for the onset of instability is visual, i.e. the visual appearance of the Dean vortices. However, visualization remains a qualitative criterion; numerically, the visualization technique depends strongly on the number of iso-value contour lines selected. In other words, one can encounter a situation with two corner vortices (no instability) for a given Dean number and a given number of iso-value contour lines, whereas for the same Dean number and under the same operating conditions, if one increases the number of iso-value contour lines, two more Dean vortices may appear near the concave wall (with instability). Experimentally, instability is signaled by the appearance of the Dean vortices, but the Dean vortices are visible only when they are highly amplified. Therefore, in both studies – numerical and experimental visualization – the critical Dean number tends to be systematically overestimated.

Instead of using visualization, a more precise criterion would be to measure the shear stresses on the concave wall. However, the modification of distribution of wall shear stresses becomes detectable by measurements only once the Dean vortices have sufficiently developed. Therefore, there would be a delay between the occurrence of instability and its detection. Nevertheless, we apply the same concept by measuring the radial gradient of the axial velocity. For this, we first locate the center of the Dean vortices for a supercritical Dean number (Fig. 7(b)) and then decrease the Dean number until the Dean vortices disappear (Fig. 7(a)). Line AA in Fig. 7(b) shows the junction between the centers of the Dean vortices. Fig. 8, which plots the radial gradient of the axial velocity ($\mathrm{d}w/\mathrm{d}y$) along line AA in Fig. 7(b), shows that for a duct of square cross-section, this gradient has a double peak at low Dean numbers and triple peaks at high Dean numbers. We choose the passage from two to three peaks as the criterion for the instability threshold. To facilitate detection of this passage, we calculate the slope of the velocity gradient along the x coordinate; for low Dean numbers the slope is canceled three times, while for high Dean numbers it is canceled five times. The same criterion

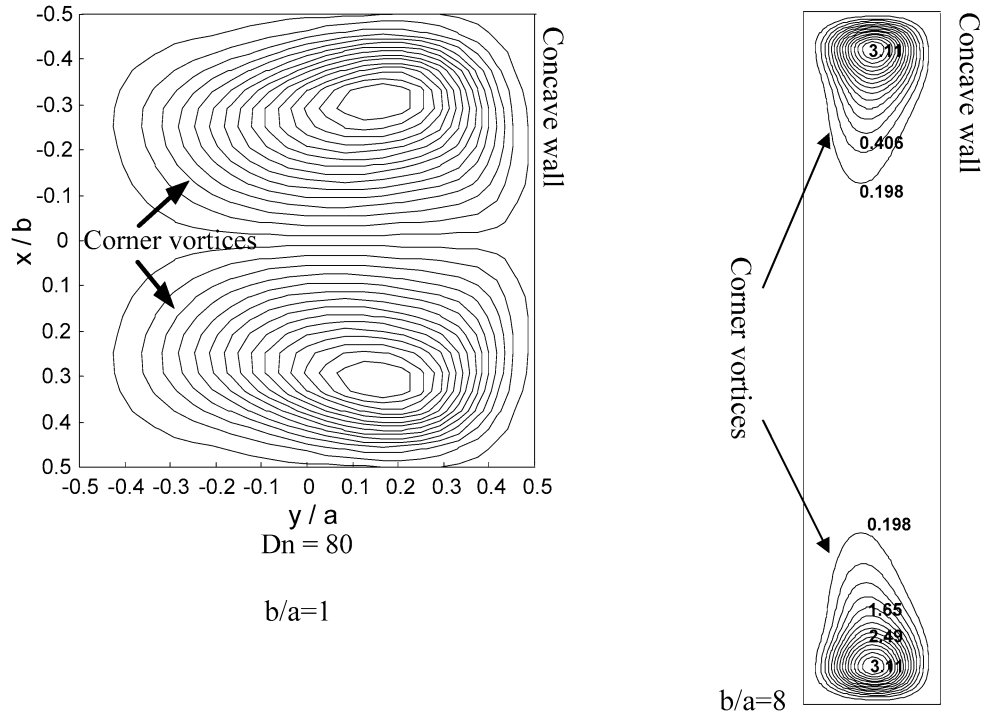

(a)

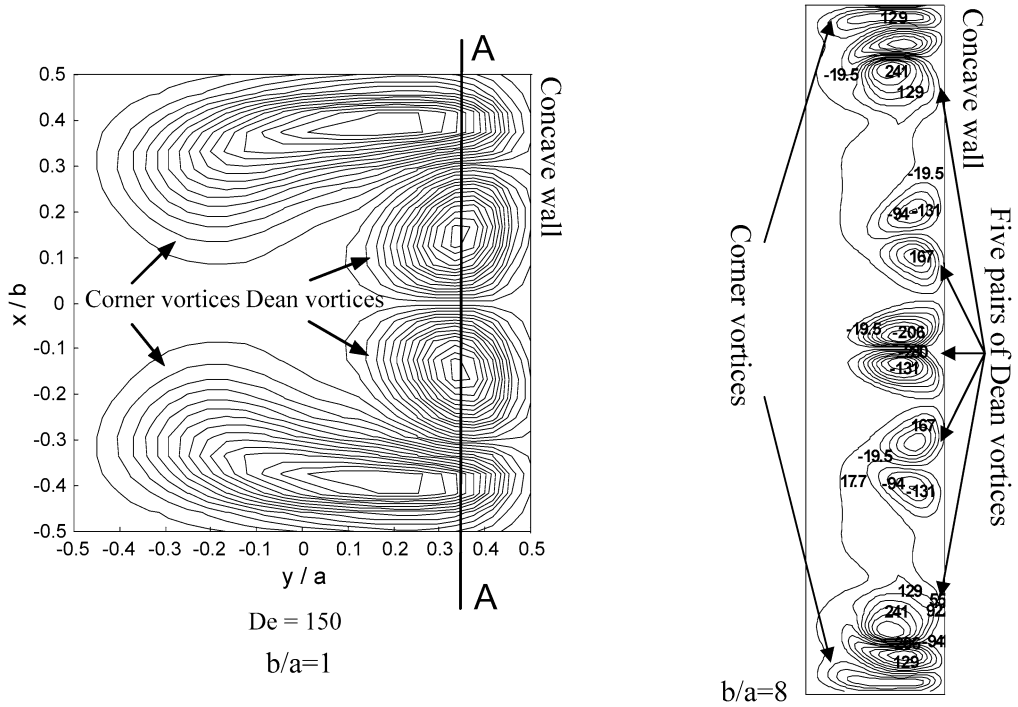

(b)

Fig. 7. Evolution of Dean roll-cells instability in rectangular curved ducts with $b/a = 1$ and 8 and $Rc/D_h = 10$. (a) Flow without Dean instability, (b) flow with Dean instability.

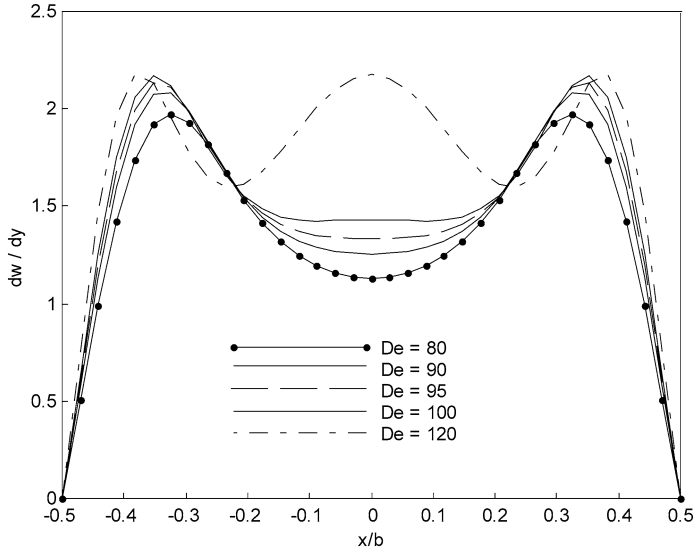

Fig. 8. Radial gradient of the axial velocity along the line AA of Fig. 7.

was used for curved channels of rectangular cross-sections of different aspect ratios, and can also be used to measure experimentally the occurrence of Dean instability.

To optimize the mesh grid, several grids were tested for a curved duct of square cross-section, ranging from 20 to 34 nodes on the flat and curved walls and from 5 to 10 mm between two successive grid surfaces. On Fig. 9 the axial velocity gradient ($\mathrm{d}w/\mathrm{d}y$) in the center of the Dean vortices (line AA in Fig. 7) is plotted for various grids, all with Dean number 110. This figure shows our mesh optimization: the number of curved wall nodes is optimized by fixing the number of nodes on the flat walls (Fig. 9(a)), and the number of flat wall nodes by fixing the number of nodes on curved walls (Fig. 9(b)). Finally, the distance between two successive grid surfaces is optimized by fixing the number of nodes in the curved and flat walls (Fig. 9(c)). Fig. 9 suggests it is reasonable to use 24 nodes on the flat and curved walls, corresponding to square meshes of 0.83×0.83 mm^2 on the surface and 10 mm between two adjacent grid surfaces.

4.3.2. Influence of the curvature ratio (Rc/D_h) on Dean instability

Much numerical and experimental work has been done on Dean instability in various configurations. For curved ducts of circular cross-section, most analyzes (Dean [6] and Ito [11]) indicate that Dean number is the primary control parameter and that curvature effects are completely contained in this parameter. Many authors (Bara et al. [25], Ghia and Sokhey [14], Hille et al. [31]) have tried to detect the critical Dean number for ducts of square cross-section, finding critical Dean numbers respectively of 137, 143, and 150. These discrepancies seem to arise from the use in all these studies of a qualitative criterion for the onset of the instability (experimental visualization or numerical path lines). In addition, the Dean number was considered the unique control parameter. As suggested above, this hypothesis is not necessarily valid: other parameters can influence the onset of instability. In this section we examine the influence of the curvature ratio on the onset of Dean instability for various aspect ratios. We present the results of our numerical study in Fig. 10 and compare them with different numerical and experimental results in the literature.

The results of the present numerical work (by using the criterion developed in Section 4.2.1) show no curvature ratio effect on the critical Dean number for aspect ratio 1, whereas for aspect ratio 8, the critical Dean number decreases rapidly when the curvature ratio increases to 10 (i.e. the instability appearance is advanced) and then becomes constant. Fig. 10 shows that the present study underestimates the critical Dean number compared to previous studies, largely because of the highly sensitive criterion adopted here compared to the qualitative one used in the literature. However, the trend is confirmed for the decreasing part of the curve, where Rc/D_h is less than 10, and for the constant part as well. A net difference is observed between the present results and those of Thangam and Hur [28], which show a variation in critical Dean number with Rc/D_h for the square section case ($b/a = 1$). However, for square cross-

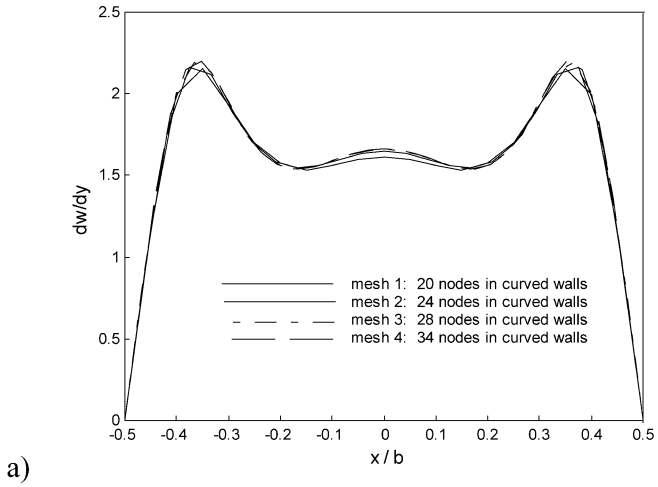

a)

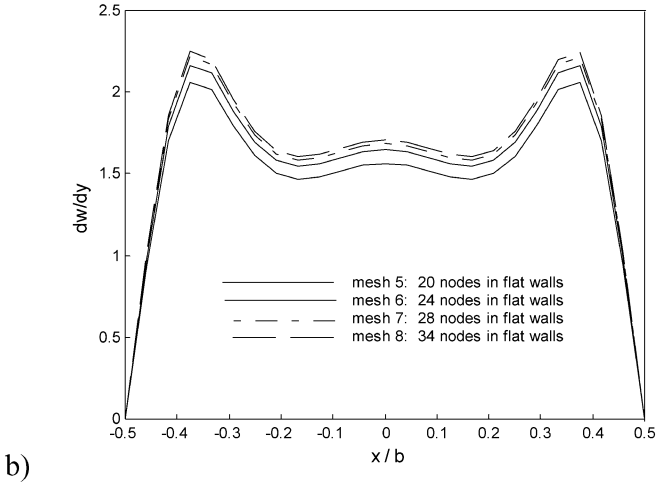

b)

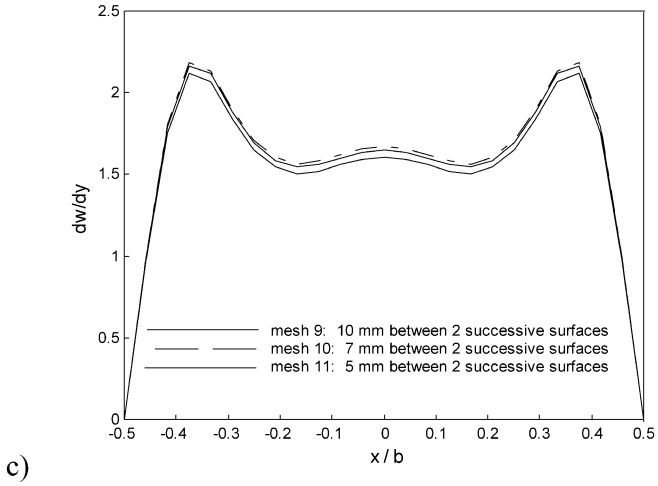

c)

Fig. 9. Optimization of mesh grid in curved square duct at $De = 110$. (a) In curved walls (the number of nodes is fixed to 24 in flat walls and 10 mm between two successive surfaces), (b) in flat walls (the number of nodes is fixed to 24 in curved walls and 10 mm between two successive surfaces), (c) between two successive surfaces (the number of nodes is fixed to 24 in curved and flat walls).

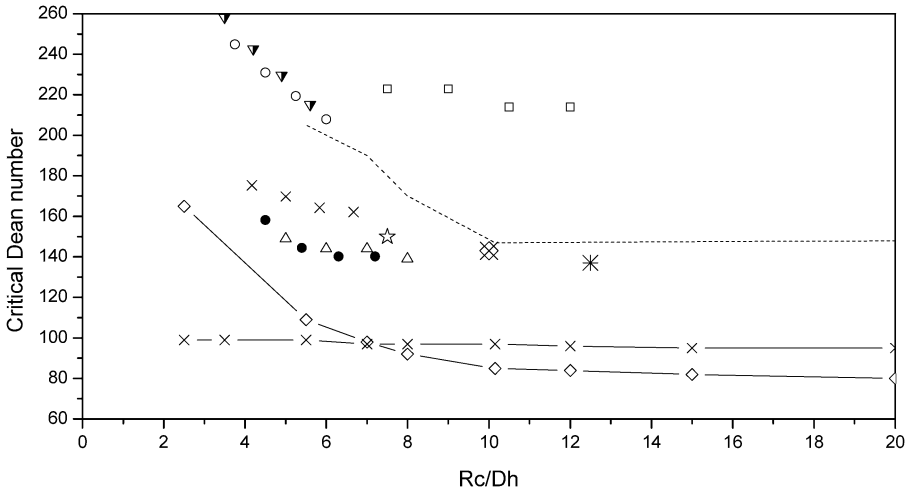

−×− Present study ($b/a = 1$), numerical study
−◇− Present study ($b/a = 8$), numerical study
□ Sugiyama et al. [21], ($b/a = 0.5$), experimental study
△ Sugiyama et al. [21], ($b/a = 1$), experimental study
● Sugiyama et al. [21], ($b/a = 1.25$), experimental study
× Sugiyama et al. [21], ($b/a = 1.5$), experimental study
○ Sugiyama et al. [21], ($b/a = 2$), experimental study
▼ Sugiyama et al. [21], ($b/a = 2.5$), experimental study
☆ Hille et al. [31], ($b/a = 1$), numerical study
✳ Bara et al. [25], ($b/a = 1$), experimental study
------ Thangam and Hur [28], ($b/a = 1$), numerical study
⊠ Hwang and Chao [15], ($b/a = 1$), numerical study

Fig. 10. Effect of curvature ratio on the Dean instability onset. The critical Dean number for square and rectangular section (respectively cross and diamond) from the present works is compared with numerical and experimental results of previous studies with different aspect ratio.

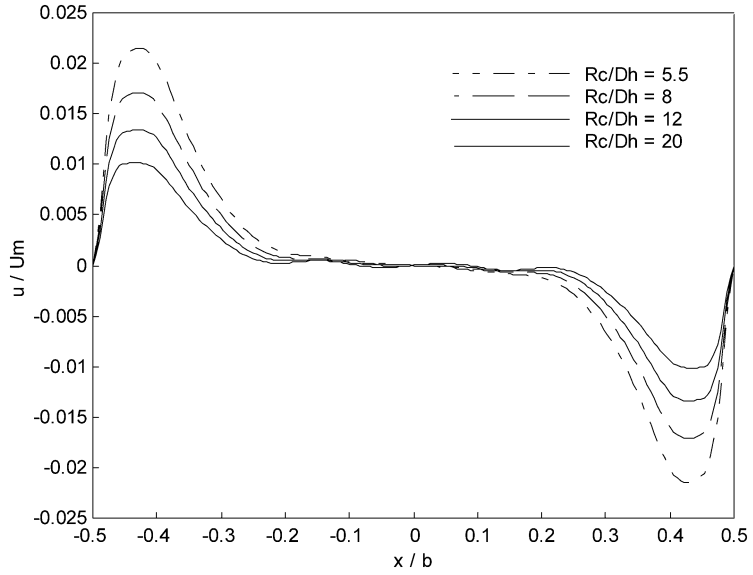

Fig. 11. Effect of curvature ratio on the flat mid-plane secondary flow velocity component (u/Um) profiles in the curved mid-plane at Dean number 90, $\theta = 180°$, $b/a = 8$.

section, the results of Sugiyama et al. [21] show a very small variation in critical Dean number in the same Rc/D_h range and seem close to our observations.

To investigate this evolution, we plot in Fig. 11 the secondary velocity component (u/Um) profile in the flat mid-plane for different curvature ratios. This figure shows that for identical Dean number, when Rc/D_h increases, the width of the central part of the velocity profile increases. This result explains the flatness of the corner vortices, which

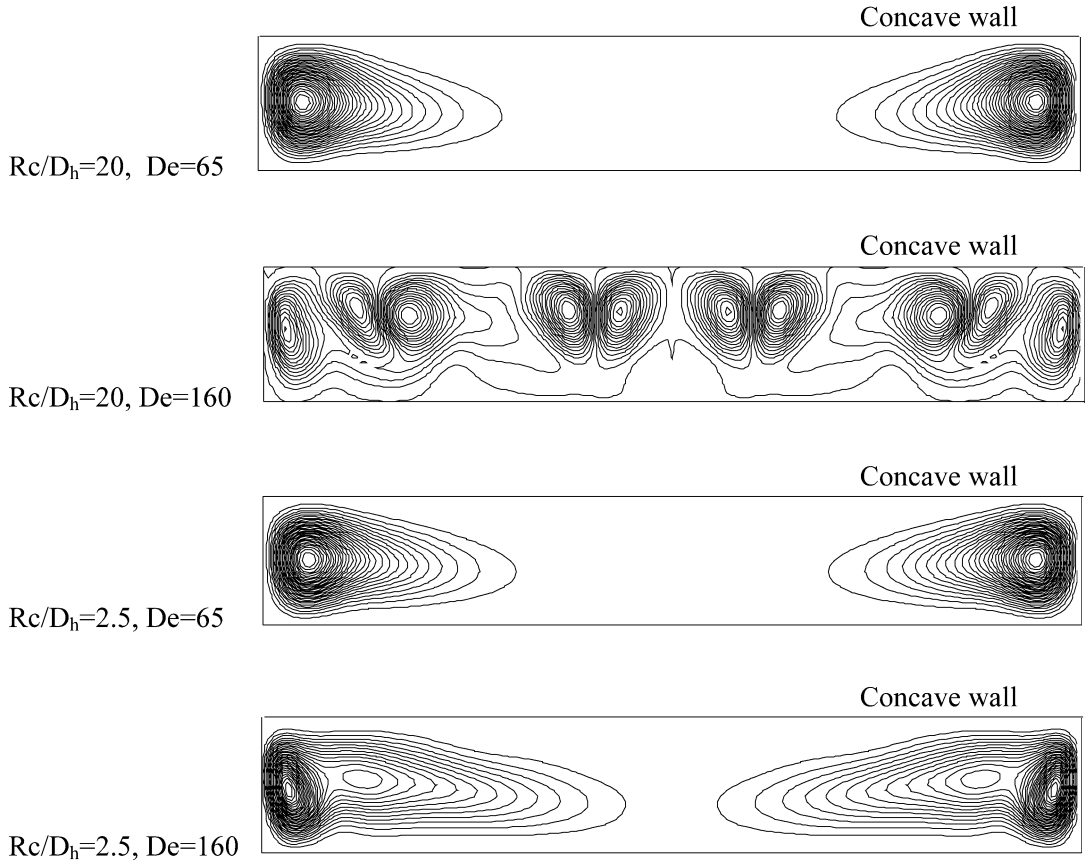

Fig. 12. Helicity contour lines, $\theta = 180°$, $b/a = 8$ and $Rc/D_h = 2.5$ and 20.

are confined more and more closely to the side walls and seem to indicate a new redistribution of energy among the flow structures, giving rise to the Dean vortices. This hypothesis is supported by Fig. 12, which shows the helicity lines corresponding to the critical Dean numbers for two values of Rc/D_h.

4.3.3. Influence of the aspect ratio on Dean instability

Here we discuss the effects of cross-section aspect ratio on Dean instability for a constant curvature ratio of 10. The evolution of the critical Dean number with aspect ratio is presented in Fig. 13, which compares the present results with those of previous studies. The trend of our curve and the values of the critical Dean numbers are globally in good agreement with the results in the literature, especially those of Cheng et al. [13] and Sugiyama et al. [21]. The apparent differences arise because of our more rigorous criterion for the onset of instability and also because the curvature ratios are different.

The variation of the critical Dean number with duct aspect ratio is noticeably less regular than the Rc/D_h effect. The critical Dean number shows a local minimum at $b/a = 1$ and increases for aspect ratios less than 1 up to 4. Beyond $b/a = 4$ it decreases and reaches a constant value at $b/a = 8$. The minimum value corresponds to curved parallel plates.

In order to better understand the implication of the aspect ratio on the evolution of the critical Dean number seen in Fig. 13, we consider the relative influence of the secondary flow strength and the confinement effect. For this purpose we show in Fig. 14 axial velocity profiles in the flat mid-plane at the exit of a 180° curved channel for $De = 55$ and for aspect ratios from 0.5 to 8. Decreasing the aspect ratio causes a stronger secondary flow that transfers high-momentum fluid toward the concave wall and transfers low-momentum fluid from near the concave wall back to the center of the channel cross-section, a phenomenon that promotes Dean instability. On the other hand, when the aspect ratio increases, confinement has a smaller effect in that the Dean vortices have more space and are freer to expand. In

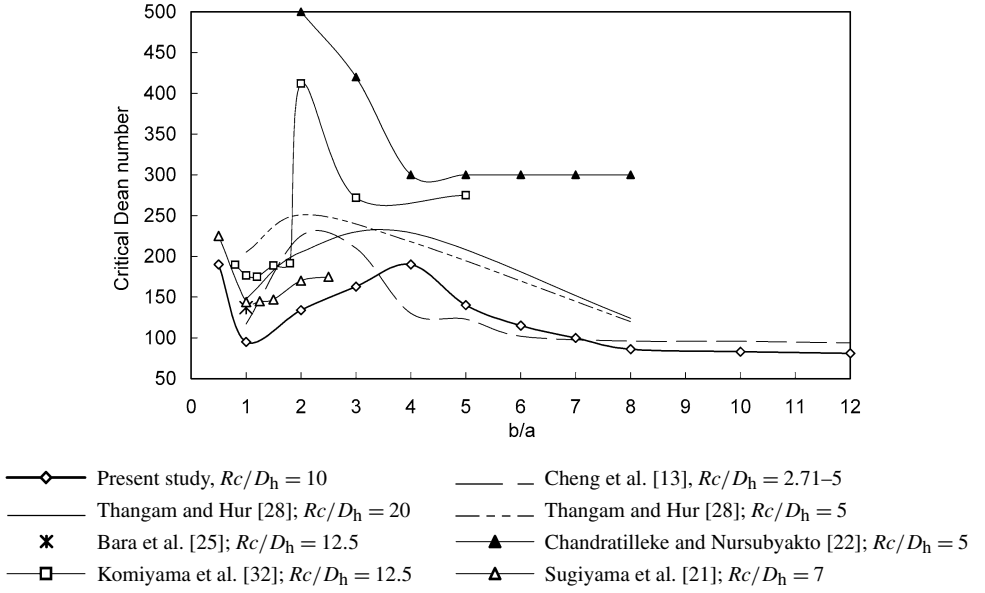

Fig. 13. Effect of aspect ratio on Dean instability.

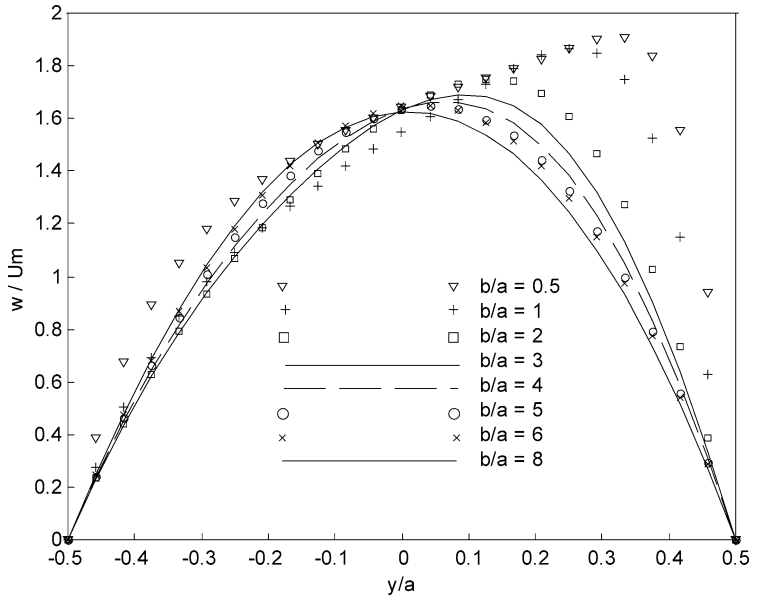

Fig. 14. Effect of aspect ratio on the axial velocity profiles along the flat mid-plane ($x = 0$) at $De = 55$, $Rc/D_h = 10$.

fact, when the Dean number and the curvature ratio are kept constant and the channel aspect ratio is increased, both the confinement effect and the resistance to secondary flow at the center of the channel cross-section decrease, i.e. it is easier to form Dean vortices, as shown in Fig. 15. Hence the occurrence of instability is advanced.

When the aspect ratio increases, these two effects compete; their relative magnitudes explain the different ranges of the critical Dean number. For a weak aspect ratio ($b/a < 1$), the confinement effect dominates and therefore increases the critical Dean number. For b/a between 1 and 8, both effects must be considered. However, for b/a from 1 to 4, the secondary flow effect dominates and consequently the critical Dean number increases, whereas for b/a from 4 to 8, the effect of non-confinement prevails and therefore the critical Dean number decreases. Above $b/a = 8$, the influence of the side walls is minimal; hence the critical Dean number decreases moderately and Dean instability becomes essentially independent of aspect ratio.

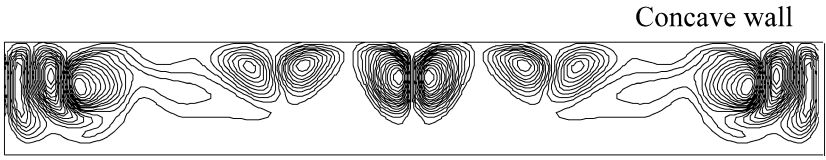

(a)

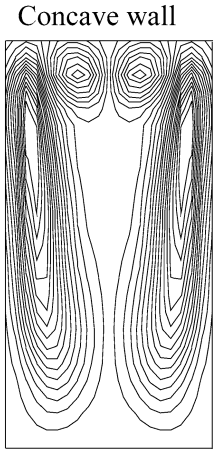

(b)

Fig. 15. Vortex organization at $De = 300$. (a) $b/a = 8$, (b) $b/a = 0.5$.

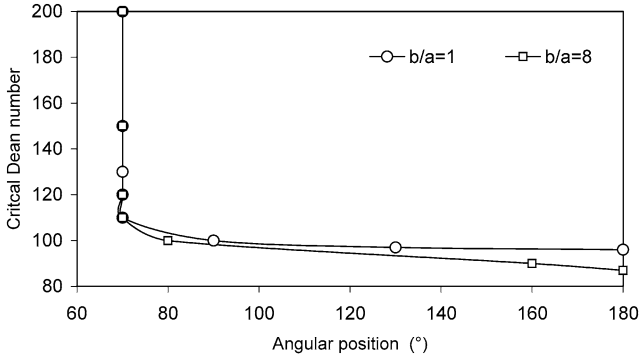

Fig. 16. Evolution of the critical Dean number with the angular position, $Rc/D_h = 10$.

4.3.4. Evolution of the critical Dean number at different angular positions

Previous sections have discussed the onset of Dean instability at the outlet section of the curved channel (180°). It is expected, however, that even for a supercritical Dean number at channel exit, flow can be sub-critical in an upstream position. The onset of Dean instability was studied at different angular positions for curvature ratio 10 and for two aspect ratios, $b/a = 1$ and 8. Fig. 16 presents the evolution of the critical Dean number with the angular position. The value of the critical Dean number was detected at each angular position. For both aspect ratios, the critical Dean number varies weakly with angular position between 80° and 180°.

The same curve shows a strong variation of the critical Dean number between 70° and 80°. This last value seems to be a limit in that we saw no onset of instability below this value.

4.3.5. Evolution of Dean instability along a curved channel

Fig. 17 plots the values of critical Dean number as a function of position in a curved channel of aspect ratio 8 and curvature ratio 10. The lower experimental curve (full line) of critical Dean number corresponds to the appearance of the first pair of Dean vortices; the upper curves correspond to two-, three- and four-pair patterns.

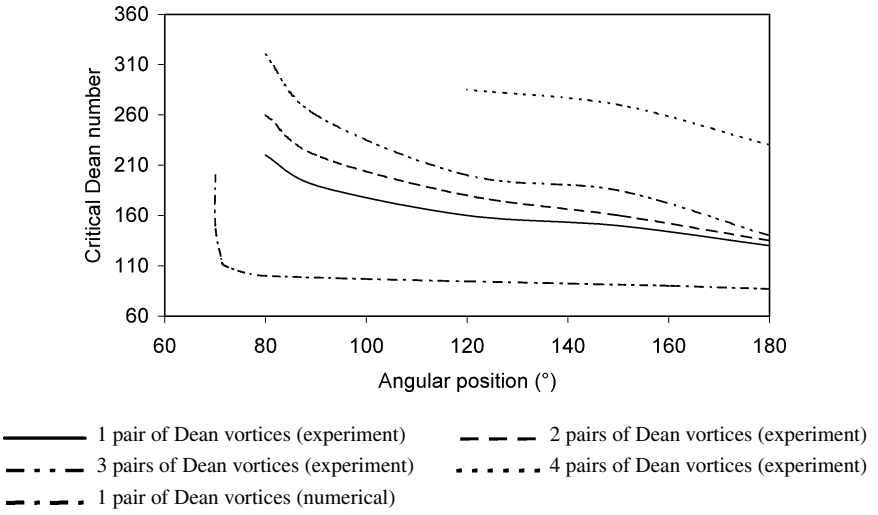

Fig. 17. Critical Dean number at different angular positions, $b/a = 8$ and $Rc/D_h = 10$.

Experimentally, the Dean instability starts at angular position 80°, and the critical Dean number decreases in the axial direction. This decrease in the critical Dean number can be explained by saying that for high Dean numbers, corresponding to high centrifugal force, a small axial length is sufficient to form Dean vortices, while for weak centrifugal force a long axial length is needed. The four-Dean-vortex instability starts only at angular position 120°. Fig. 17 also plots the numerical results corresponding to the critical Dean number for the appearance of the first vortex pair. As expected, the critical Dean number values are below the experimentally obtained critical Dean numbers. As remarked previously, this is due to the use in this study of a quite sensitive numerical criterion for the detection of the instability threshold compared to the experimental visual criterion.

4.4. Global flow characterization

Since it is the global flow which governs the transport phenomena, once the onset of Dean instability is detected it is important to study the behavior of the global flow, i.e. the basic flow in the sub-critical regime and the basic flow together with the instability effects in the super-critical regime.

The global flow for Dean numbers 80 and 150 is represented by helicity contour lines on Fig. 7 for square and rectangular ($b/a = 8$) curved ducts. The curvature ratio is maintained constant and equal to 10 and the helicity contour lines are represented at the duct exit ($\theta = 180°$).

At Dean number 80, the flow is formed of two counter-rotating vortices for the two duct cross-sections. For the rectangular cross-section ($b/a = 8$), the two corner vortices are confined near the flat walls. For Dean number 150, the flow contains four vortices in the square cross-section: two corner vortices close to the flat walls and two Dean vortices in the central part of the concave wall. In the rectangular cross-section ($b/a = 8$), Dean instability takes the form of several vortices distributed on the concave wall.

The velocity field and the development of the secondary flow depend on several parameters: the Reynolds number, the curvature ratio Rc/D_h, the development length, the aspect ratio b/a, and the nature of velocity profile at the inlet boundary. In this study, a fully developed Poiseuille flow velocity profile is imposed at the duct entrance. Section 4.4.1 discusses the influence of the Dean number on velocity distribution and Section 4.4.2 addresses the influence of the cross-section aspect ratio on the development length.

4.4.1. Influence of Dean number on the velocity distribution

Fig. 18 shows the effect of Dean number on the axial velocity profile in a curved channel of square cross-section, for curvature ratio 10. Velocity profiles are plotted on two perpendicular planes: the flat mid-plane parallel to the flat walls (Fig. 18(a)) and the curved mid-plane parallel to the curved walls (Fig. 18(b)). In Fig. 18(a) the increase in the Dean number shifts the peak of the axial velocity profile toward the concave wall, thus increasing the transfer of axial momentum from the center to the concave wall. The imbalance at the concave wall between the pressure gradient

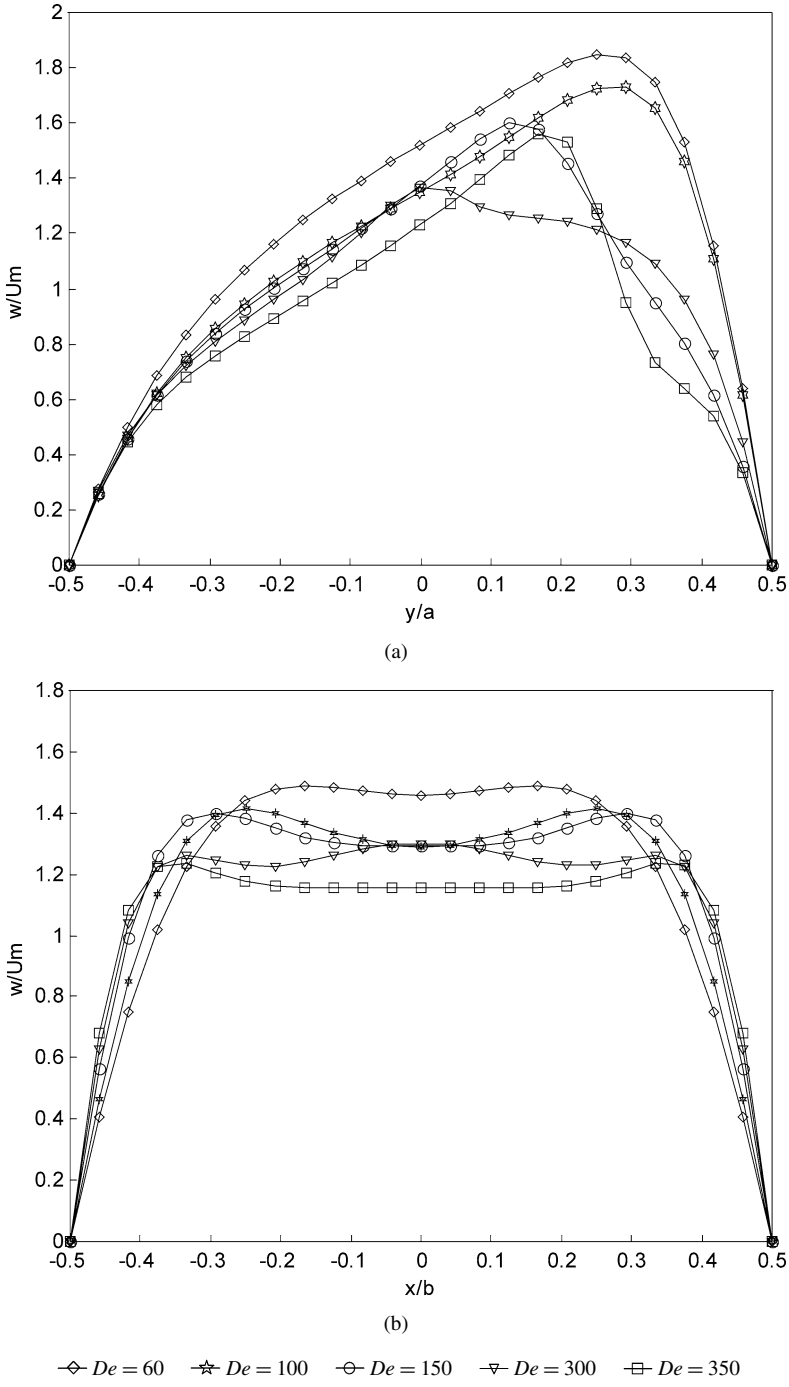

Fig. 18. Effect of Dean number on the axial velocity profiles, $\theta = 180°$, $b/a = 1$ and $Rc/D_h = 10$. (a) Flat mid-plane ($x = 0$), (b) curved mid-plane ($y = 0$).

(acting toward the center of curvature) and the centrifugal force (acting toward the concave wall) causes the formation of corner vortices.

As this transfer becomes stronger, however, the viscous effect can no longer hold the two corner vortices. Dean vortices bring the fluid from the concave wall to the center and thus decrease the fluid transfer toward the concave wall. Up to the critical Dean number, the peak of the axial velocity profile (Fig. 18(a)) decreases and migrates continuously

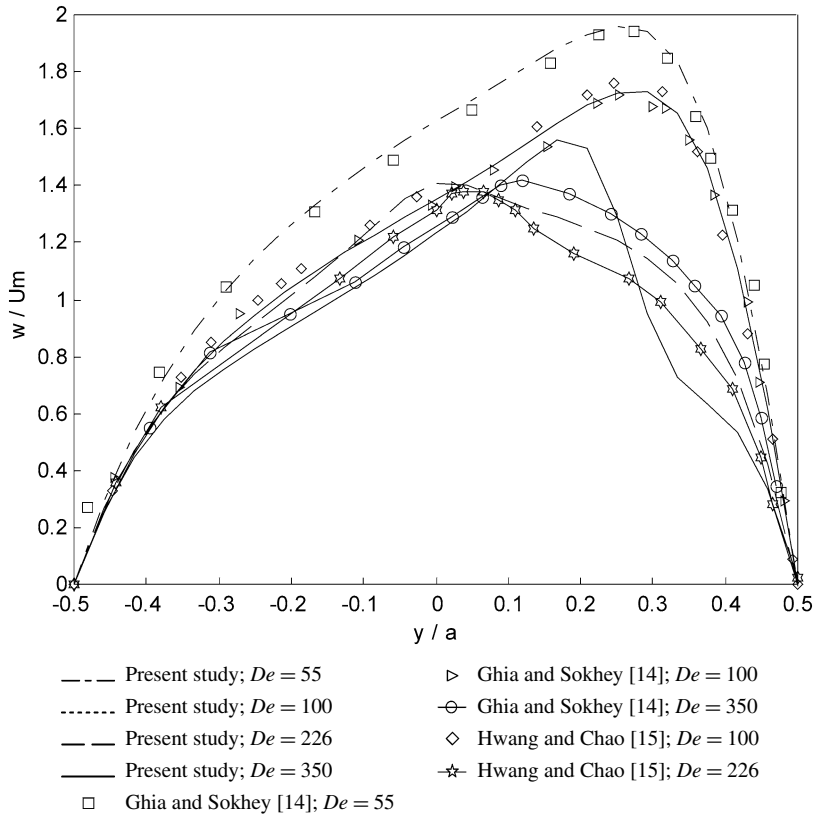

Fig. 19. Comparison with the literature of the effect of Dean number on the axial velocity profiles in the flat mid-plane ($x = 0$), $\theta = 180°$, $b/a = 1$ and $Rc/D_h = 10$.

toward the section center. For high Dean numbers, this peak makes another shift to the concave wall because of the increasing centrifugal force. In the mid-plane parallel to the flat walls (Fig. 18(b)), the loss of axial momentum near the concave wall caused by the Dean instability is absorbed in the section center, causing the formation of the third peak. This third peak then disappears for higher Dean numbers, corresponding to the second shift of the peak of the axial velocity profile toward the concave wall, as shown in Fig. 18(a) for $De = 350$. On Fig. 19 the present results are compared with those of the literature for $Rc/D_h = 10$. One notices that for low Dean numbers (55 and 100) present results are in good agreement with the results of Ghia and Sokhey [14] as well as Hwang and Chao [15]. The more one increases the Dean number the more the results deviate from those of previous authors. Nevertheless, the evolution of the position of the profile maximum follow the same trend as the results of Ghia and Sokhey [14] and of Hwang and Chao [15]. The discrepancy among the results, especially at $De = 350$ can be attributed to the fact that the results of the present study correspond to a developing Dean flow whereas the velocity profiles of Ghia and Sokhey [14] are plotted for a fully developed Dean flow. One can expect that in their fully developed state the present results match better those of Ghia and Sokhey [14].

Fig. 20 shows, in the curved mid-plane, the distribution of the two non-dimensional secondary flow components (u/Um and v/Um) with increasing Dean number for a square cross-section channel ($Rc/D_h = 10$). In Fig. 20(a), the x-wise component of the secondary velocity (u/Um) shows two peaks, for Dean numbers 60 and 100, that correspond to the centers of the two corner vortices and move toward the flat walls as the Dean number increases from 60 to 100. Hence the resistance to Dean vortex formation decreases. For these two Dean numbers, the y-wise component of the secondary velocity (v/Um) has three peaks (Fig. 20(b)). The peak in the center of the section corresponds to the radial pumping action of the two corner vortices. From Dean number 100, new inflection points appear that indicate the structure modification of the secondary flow. Fig. 20(a) shows a drastic change between $De = 60$ and 100 in which we observe two peaks, and $De \geqslant 150$ in which two additional peaks appear due to the appearance of Dean instability. The maximum value of u component of the velocity changes sign and its amplitude increases gradually. However, from

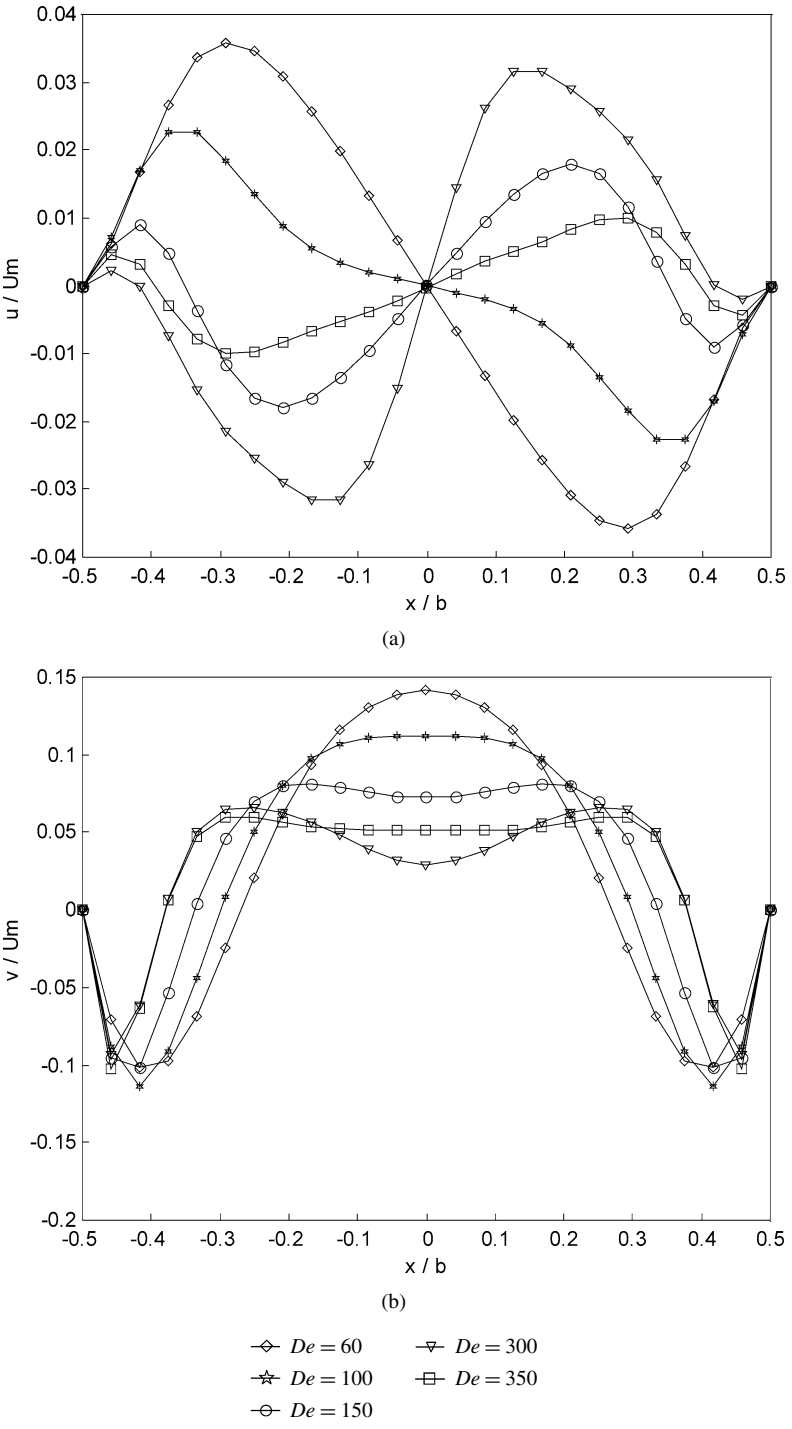

Fig. 20. Effect of Dean number on secondary flow velocity profiles in the curved mid-plane, $\theta = 180^\circ$, $b/a = 1$ and $Rc/D_h = 10$. (a) Flat mid-plane component (u/Um), (b) curved mid-plane component (v/Um).

$De = 300$ one observes a reduction of the maximum amplitude as seen for $De = 350$. This reduction is mainly due the displacement of the center of Dean vortices toward the concave wall as shown on Fig. 21. Due to this containment of the Dean vortices close to the concave wall the quantity of the low momentum fluid particles injected to the center of

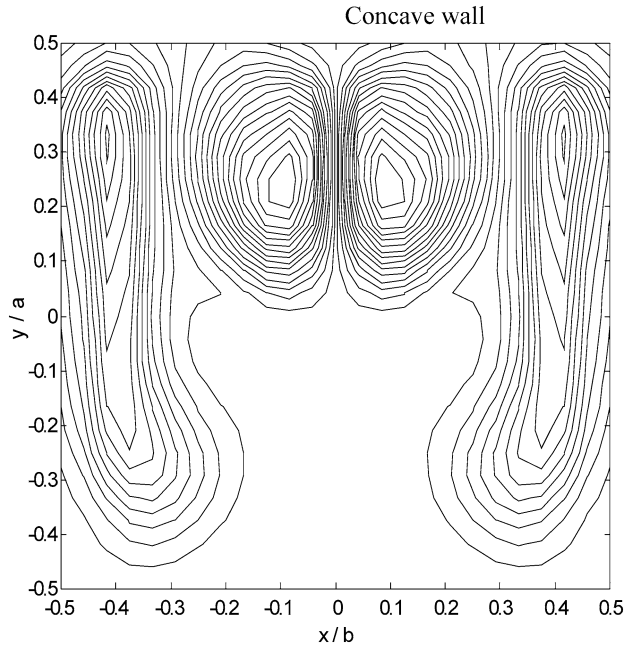

(a)

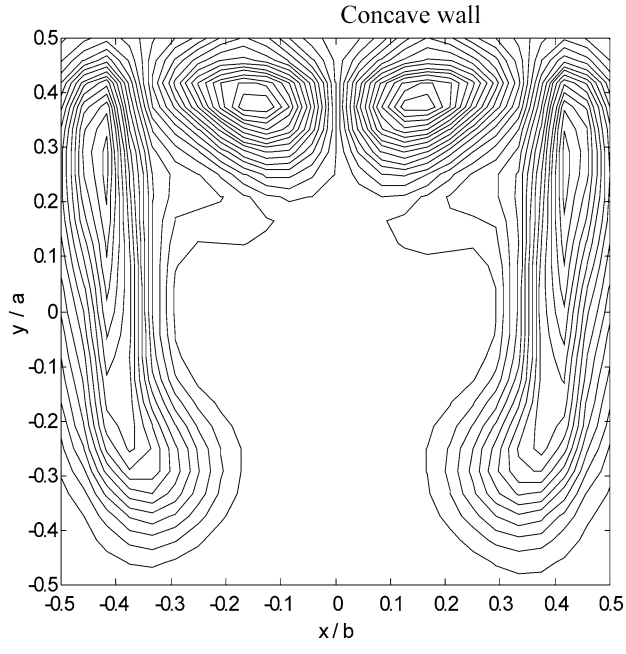

(b)

Fig. 21. Dean vortices, $Rc/D_h = 10$. (a) $Dn = 300$, (b) $Dn = 350$.

the duct section by the Dean vortices is reduced and therefore, the valley on the v-component curve for $De = 300$ is transformed to a plateau for $De = 350$ (Fig. 20(b)).

The study described above was also carried out for a rectangular cross-section of various aspect ratios. Fig. 22 shows the axial velocity profiles for aspect ratio 8. We see that for sub-critical Dean numbers the shift in the axial velocity profile (in the flat mid-plane, Fig. 22(a)) towards the concave wall that was present in the square section does

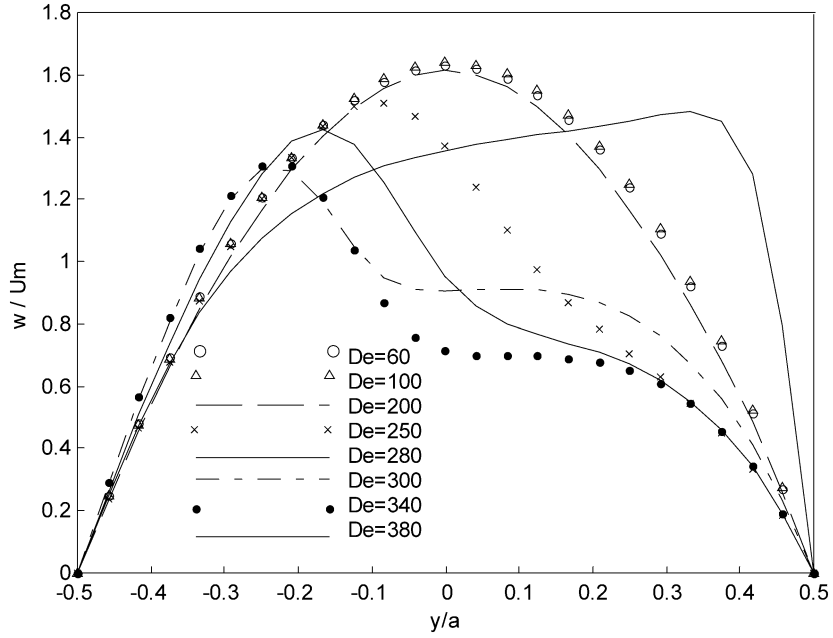

(a)

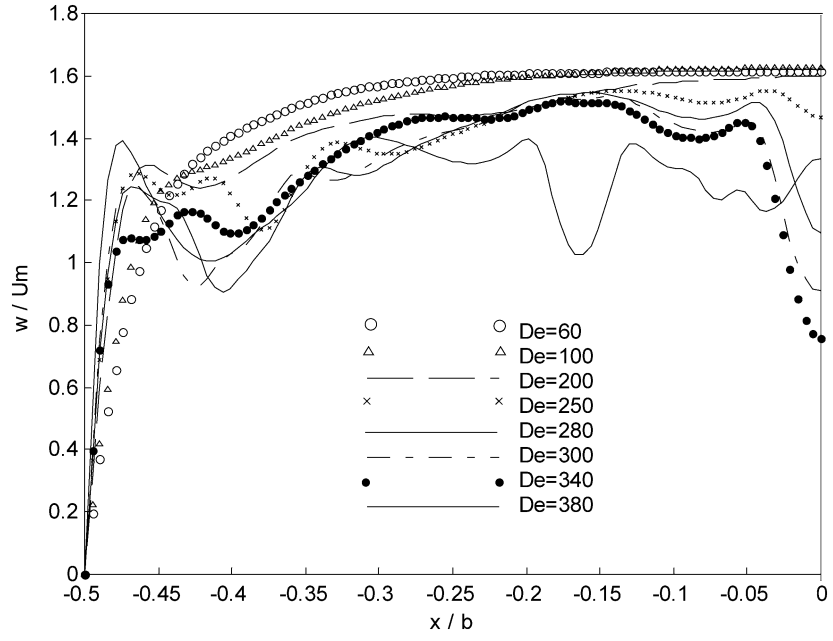

(b)

Fig. 22. Effect of Dean number on axial velocity profiles, $\theta = 180°$, $b/a = 8$ and $Rc/D_h = 10$. (a) Flat mid-plane ($x = 0$), (b) curved mid-plane ($y = 0$).

not occur, and the velocity profile in the curved mid-plane does not have the same two-peak form. For super-critical Dean numbers, the axial velocity profile in flat mid-plane shifts excessively towards the convex wall.

In the curved mid-plane ($y = 0$), the axial velocity profile is uniform for $De = 60$ in the channel center. The onset of instability is signaled by deformation of the velocity profiles in the center of the cross-section, with the appearance of weak velocity zones represented by peaks and valleys. The valleys correspond to the up-wash zones of Dean vortices in which the vortices pump low-momentum fluid from the concave wall vicinity to the center. The peaks correspond

to down-wash zones in which the Dean vortices push high-momentum fluid from the center toward the concave wall; the amplitude of these peaks increases with Dean number.

4.4.2. Influence of the aspect ratio on development length

The axial developed length, is the distance from the duct entrance beyond which the axial velocity profiles do not vary anymore. Bara et al. [25] and Ghia and Sokhey [14] studied the axial development in curved channels of square cross-section, respectively for a parabolic and a flat inlet velocity profile. The axial development length for channels of square cross-section and rectangular section ($b/a = 8$) is shown in Fig. 23. The evolution of axial development length with Dean number is linear. The results of the present study agree well with those of Bara et al. [25]. The axial development length in the study of Ghia and Sokhey [14] is more significant because of the nature of the inlet conditions. Austin and Seader [33] showed that, for a curved duct of circular cross-section, the axial length required to reach a fully developed flow is more significant when the inlet profile is flat than when it is parabolic. In the present work the axial development lengths can be roughly obtained from the following correlations derived from Fig. 23:

– for curved ducts of square cross-section

$$\frac{\theta}{180} = 0.7De + 0.206;$$

– for curved ducts of rectangular cross-section ($b/a = 8$)

$$\frac{\theta}{180} = 0.7De + 0.139.$$

Fig. 23 shows also that the axial development length is longer for square curved channels. Muchnik et al. [26] have shown experimentally that the axial development length in a straight channel is larger for $b/a = 1$ than $b/a = 8$. The reduction of the side-wall effect reduces the axial developed length.

However, it should be noticed that basing on the axial velocity profiles (in the flat mid-plane) as a criterion for flow development can be misleading. In fact, on Fig. 23 one observes that the basic flow for the case of $b/a = 8$ is developed, for example for $De = 90$, at the angular position about 90° showing no sign of the existence of the Dean vortices at this position. While, Fig. 16, using the criterion for the onset of instability developed in this work, shows that for this Dean number (90) at angular position 90° the Dean instability has already been triggered. This confirms once again appropriateness of the criterion developed here.

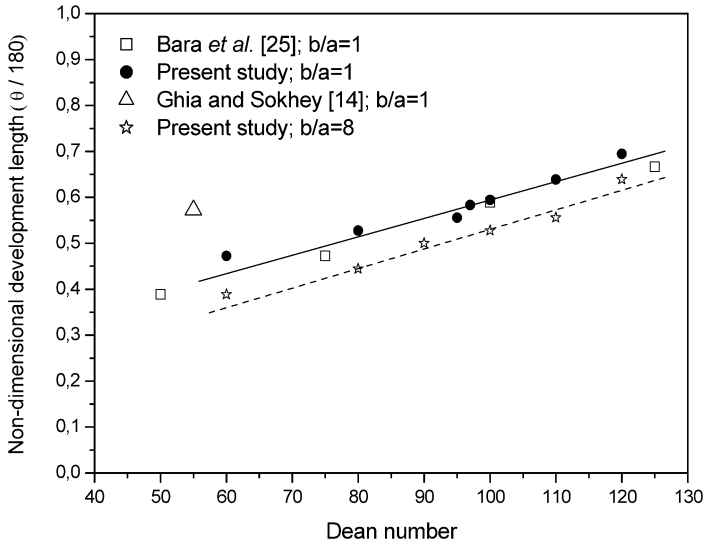

Fig. 23. Axial development length in curved channels as a function of Dean number, $Rc/D_h = 10$.

5. Conclusions

We studied Dean instability in curved channels of rectangular cross-section numerically and experimentally. The experimental study was carried out in a curved channel of aspect ratio 8 and curvature ratio 10 and was extended numerically to various other aspect ratios and curvature ratios.

An accurate numerical criterion based on the radial gradient of the axial velocity was defined that allows detection of the Dean instability threshold. Prediction of the critical Dean number by this criterion lets us detect the instability closer to its onset than in previous work.

The effects of the curvature ratio and aspect ratio on Dean instability were studied numerically. In particular, we show that the critical value of the Dean number decreases with increasing curvature ratio. The variation of the critical Dean number with aspect ratio is less regular.

Flow visualizations were made in the laminar flow of a Newtonian fluid in a 180° curved rectangular channel of aspect ratio 8 and curvature ratio 10. Additional counter-rotating pairs of vortices were observed and the development of the unstable flow vortices becomes clear. A relation between the critical Dean number and axial position in the curved channel is proposed.

References

[1] H. Peerhossaini, On the effects of streamwise vortices on wall heat transfer, in: R. Shah (Ed.), Compact Heat Exchangers for Process Industry, Begell House Publishers, New York, 1997, pp. 571–589.
[2] C. Castelain, A. Mokrani, Y. Le Guer, H. Peerhossaini, Experimental study of chaotic advection regime in a twisted duct flow, Eur. J. Mech. B Fluids 20 (2001) 205–232.
[3] H.K. Moffatt, Viscous and resistive eddies near a sharp corner, J. Fluid Mech. 48 (1) (1964) 1–18.
[4] W.H. Finlay, K. Nandakumar, Onset of two-dimensional cellular flow in finite curved channels of large aspect ratio, Phys. Fluids A 2 (7) (1990) 1163–1174.
[5] S.A. Berger, L. Talbot, L.S. Yao, Flow in curved pipes, Annu. Rev. Fluid Mech. (1983) 461–512.
[6] W.R. Dean, Note on the motion of fluid in a curved pipe, Philos. Mag. 4 (1927) 208–223.
[7] J. Eustice, Experiments of streamline motion in curved pipes, Proc. Roy. Soc. London Ser. A 85 (1) (1911) 19–31.
[8] C.M. White, Streamline flow through curved pipes, Proc. Roy. Soc. Ser. A 123 (1929) 645–663.
[9] H. Ito, Theory on laminar flows through curved pipes of elliptic and rectangular cross sections, Rep. Inst. High Speed Mech., Tohoku Univ., Sendai Japan, 1, 1951, pp. 1–16.
[10] H.G. Cuming, The secondary flow in curved pipes, communicated by Professor A.A. Hall, Aeronaut. Res. Counc., Reports and Memoranda N° 2880, February 1952.
[11] H. Ito, Laminar flow in curved pipes, Rep. Inst. High Speed Mech., Tohoku Univ., Sendai, Japan, 22 (224), 1970, pp. 161–180.
[12] Y. Mori, Y. Uchida, T. Ukon, Forced convective heat transfer in curved channel with a square cross section, Int. J. Heat Mass Transfer 14 (11) (1971) 1787–1800.
[13] K.C. Cheng, R.C. Lin, J.W. Ou, Fully developed laminar flow in curved rectangular channels, J. Fluids Engrg. (1976) 41–48.
[14] K.N. Ghia, J.S. Sokhey, Laminar incompressible viscous flow in curved ducts of rectangular cross-section, Trans. ASME I: J. Fluids Engrg. 99 (1977) 640–648.
[15] G.J. Hwang, C.-H. Chao, Forced laminar convection in a curved isothermal square duct, Trans. ASME J. Heat Transfer 113 (1991) 48–55.
[16] B. Joseph, E.P. Smith, R.J. Adler, Numerical treatment of laminar flow in helically coiled tubes of square cross section. Part. 1 Stationary helically coiled tubes, AIChE J. 21 (1975) 965–974.
[17] K.C. Cheng, M. Akiyama, Laminar forced convection heat transfer in curved rectangular channels, Int. J. Heat Mass Transfer 13 (1970) 471–490.
[18] J.A. Baylis, Experiments on laminar flow in curved channels of square section, J. Fluid Mech. 48 (3) (1971) 417–422.
[19] J.A.C. Humphrey, A.M.K. Taylor, J.H. Whitelaw, Laminar flow in a square duct of strong curvature, J. Fluid Mech. 83 (1977) 509–527.
[20] K.C. Cheng, J. Nakayama, M. Akiyama, Effect of finite and infinite aspect ratios on flow patterns in curved rectangular channels, in: Flow Visualisation International Symposium, Tokyo, October 1977, p. 181.
[21] S. Sugiyama, T. Hayashi, K. Yamazaki, Flow characteristics in the curved rectangular channels (visualisation of secondary flow), Bull. JSME 26 (216) (1983) 964–969.
[22] T.T. Chandratilleke, Nursubyakto, Numerical prediction of secondary flow and convective heat transfer in externally heated curved rectangular ducts, Int. J. Thermal Sci. 42 (2003) 187–198.
[23] P.M. Ligrani, R.D. Niver, Flow visualization of Dean vortices in a curved channel with 40:1 aspect ratio, Phys. Fluids 31 (1988) 3605–3617.
[24] P.M. Ligrani, S. Choi, A.R. Schallert, P.E. Skogerboe, Effect of Dean vortex pairs on surface heat transfer in curved channel flow, Int. J. Heat Mass Transfer 39 (01) (1996) 27–37.
[25] B. Bara, K. Nandakumar, J.H. Masliyah, An experimental and numerical study of the Dean problem: flow development towards two-dimensional multiple solutions, J. Fluid Mech. 244 (1992) 339–376.
[26] G.F. Muchnik, S.D. Solomonov, A.R. Gordon, Hydrodynamic development of laminar velocity field in rectangular channels, Fizicheskii Zh. 25 (4) (1973) 671–675.

[27] H. Peerhossaini, J.E. Wesfreid, On the inner structure of Görtler vortices, Int. J. Heat Fluid Flow 9 (1988) 12–18.
[28] S. Thangam, N. Hur, Laminar secondary flows in curved rectangular ducts, J. Fluid Mech. 217 (1990) 421–440.
[29] W.H. Reid, On the stability of viscous flow in a curved channel, Proc. Roy. Soc. London Ser. A 244 (1958) 186–198.
[30] M.A. Dean, Fluid motion in curved channel, Proc. Roy. Soc. Ser. A 121 (1928) 402–420.
[31] P. Hille, R. Vehrenkamp, E.O. Schulz-Dubois, The development and structure of primary and secondary flow in a curved square duct, J. Fluid Mech. 151 (1985) 219–241.
[32] Y. Komiyama, F. Mikami, K. Okui, T. Hori, Laminar forced convection heat transfer in curved channels of rectangular cross-section, Trans. ASME J. Heat Transfer B 50 (450) (1984) 424–434.
[33] L.R. Austin, J.D. Seader, Fully developed viscous flow in coiled circular pipes, AICHE J. 19 (1) (1971) 85–94.